Numerical simulation on the mechanical behavior of ecological brick masonry

Dabdon C. Nascimento[1], Francielly L. Casas[1], Fernanda Valim[1], Lucas R. dos Santos[1], White J. dos Santos[1], Rodrigo Barreto Caldas[1]

[1]*Programa de Pós-Graduação em Engenharia das Estrutura (PROPEEs),*
Universidade Federal de Minas Gerais (UFMG)-
Av. Pres. Antônio Carlos, 6627 - Pampulha,
Belo Horizonte - MG, 31270-901
dabdoneng@ufmg.br, franciellylascasas@ufmg.br,
favalim2@ufmg.br, lucas@dees.ufmg.br, white.santos@demc.ufmg.br, caldas@dees.ufmg.br

Abstract. Soil-cement brick masonry structures have gained prominence in developing countries due to their practicality, low cost and excellent ecologically sustainable alternative. However, the literature presents few numerical studies on masonry structures in soil-cement bricks, since most of the studies carried out focus on concrete and ceramic bricks. The experimental analysis was carried out by performing compression tests on small existing walls made of bricks and mortars. The objective of this study, therefore, is to present a numerical validation study carried out in ABAQUS, which uses the finite element method. For a better representation, micromodeling of the parts was used, characterized by the individual representation of the bricks and mortars and the contact interfaces between them. The numerical results were compared to the experimental results and were quite convergent, and the present study allowed us to adequately replicate the concentration of damage in the bricks, corroborating what was observed in the experimental tests.

Keywords: Soil Cement; Structural Masonry; Finite Element Method.

1 Introduction

Soil masonry is one of the most rudimentary and widely used construction methods throughout history [1]. In this scenario, the construction of soil-cement masonry has become a topic of increasing interest due to its high levels of sustainability, good mechanical strength and durability [2][3].

Compressive strength is a basic indicator of the mechanical behavior of masonry elements, since masonry is generally subjected to more intense vertical loads than horizontal ones, produced by wind and earthquakes [4]. Numerical modeling plays an important role in the structural analysis of soil-cement masonry, since testing masonry elements requires cost, time and appropriate machinery. However, the literature presents few numerical studies of soil-cement masonry structures under compression [5][6], with most studies focused on concrete and ceramic bricks.

Considering this context, the objective of this work is to present the calibration of numerical models of small soil-cement brick walls laid with flexible adhesive mortar type ACIII, based on the experimental results developed at the Multiuser Center for Experimental Analysis of Structures (CEMAEES) of the Federal University of Minas Gerais. The walls are modeled using the detailed micromodeling approach developed in the finite element program

ABAQUS CAE, version 2014. This numerical study was basically divided into two stages: general aspects of the experimental tests and calibration of the numerical model of the small walls. With the results of the numerical modeling, a study was carried out to compare the mechanisms responsible for the failure with the behavior observed during the tests.

2 General aspects of experimental tests

The experimental results used for the calibration and validation of the numerical model were based on tests developed at the Laboratory of Experimental Analysis of Structures of the Federal University of Minas Gerais. The tests consisted of the characterization of the materials that make up the model and the axial compression of small soil-cement structural masonry walls.

2.1 Characterization of the mechanical properties of materials

Compressive strength (f_c) and tensile strength (f_t) are the basic parameters for the calibration of a numerical model. For bricks, compressive strength was evaluated according to the German standard DIN 18945 [7], and uniaxial tensile strength of the bricks was determined through the three-point bending test, regulated by the European standard EN 772-6 [8], being adopted as 50% of the flexural strength, based on the studies of Huamani et al. [6]. The small walls were laid with joints of flexible adhesive mortar type ACIII, from the manufacturer Quartzolit; the characterization of the mechanical properties of the mortars was carried out according to the Brazilian standard NBR 13279 [17]. Table 2 shows the resistant capacity of the materials.

2.2 Axial compression of small walls

The small soil-cement walls were built with 11 rows of bricks, laid in tie-in mortar, with an average thickness of the horizontal joints of 7.03 mm and of the vertical joints of 12.5 mm. The soil-cement bricks had average dimensions of 70 x 126.5 x 250 mm (Figure 1), and half bricks of 70 x 126.5 x 123 mm, both with vertical holes of 56 mm (Figure 1-a). The structural behavior of the soil-cement masonry laid with adhesive mortar was evaluated through six small walls whose average dimensions are shown in Figure 1-b.

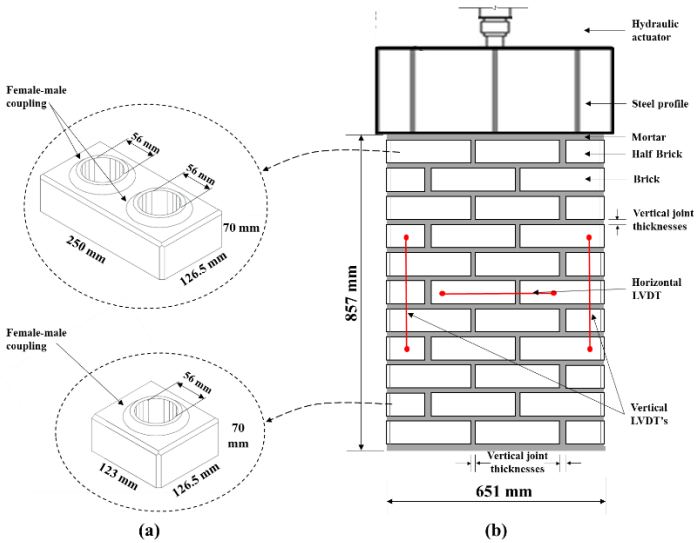

Figure 1. Compression test on small walls: (a) brick geometry; (b) geometry of small walls

Given the lack of specific standards for testing small soil-cement masonry walls, the tests were performed based on the requirements of standard NBR 16868-3 [11]. In this context, the compression tests of the small walls proposed in the experimental study were performed in a rigid reaction frame, with the loads applied to a steel

profile through a manual hydraulic actuator. In order to obtain the deformability parameters of the masonry, three Linear Variable Differential Transducers (LVDTs) were positioned: two parallel and one perpendicular to the direction of load application, all at a distance of 300 mm (Figure 1-b).

3 General aspects of numerical modeling

The numerical modeling was developed using the Finite Element Method (FEM) through the ABAQUS/Explicit software, version 6.14, employing a quasi-static resolution technique. The numerical simulation of the structural behavior of the masonry was performed with a detailed micromodeling approach. Detailed micromodeling consists of individual modeling of the bricks, mortar joints and interface between the materials [12].

3.1 Geometries, types of elements, mesh, boundary and loading condition

Due to the complexity of the actual brick geometry, which could cause non-conformity problems in the mesh, the modeling of the soil-cement bricks was simplified. The vertical chamfers at the ends of the wall were disregarded. In addition, the female-male coupling system between the units was disregarded, as it does not exert significant influence on axial compression analyses of the small walls. Figure 2-a shows the geometry of the numerical model of the small walls, as well as its parts. The external dimensions of the numerical model are 65 x 855 x 126.5 mm, with vertical holes of 56 mm in diameter, horizontal joint thickness of 7 mm and vertical joints of 10 and 15 mm (Figure 2-b). The parts (brick and mortar) were simulated using an eight-node linear solid element (C3D8), with three translational degrees of freedom at each node. To minimize irregularities in the mesh and avoid regions with distorted finite elements, the mesh was uniformized by partitioning the geometry. The lines shown in Fig. 2-b indicate the locations where partitions were created for node coincidence in the finite element mesh discretization. To achieve a balance between computational accuracy and time, a mesh convergence study was conducted to determine the appropriate mesh size. The adopted mesh size was 15 mm.

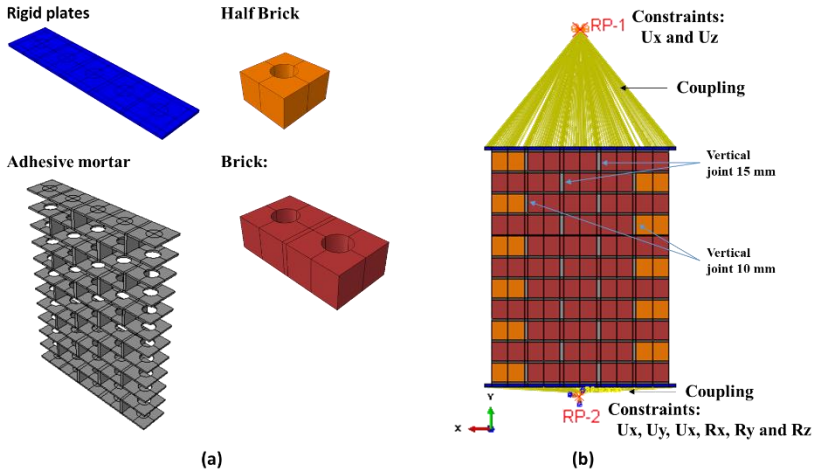

Figure 2. Numerical analysis model: (a) model parts; (b) complete model

For the small walls, two rigid plates were modeled for the upper and lower ends. Two reference points were created in the model (named RP-1 and RP-2), positioned respectively at the top and bottom of the small wall (Figure 2-b). These points were coupled to the rigid plates to evenly distribute the compressive loading and the constraints imposed on the reference points. RP-1 was constrained regarding the displacement in the XZ plane (Ux and Uz), while RP-2 was constrained regarding all degrees of freedom (Ux, Uy, Uz, Rx, Ry and Rz). To simulate the loading of the experimental analysis, a quasi-static point displacement of 6 mm was applied to RP-1. For the convergence criterion, a limit value of 5-10% was established for the ratio of kinetic energy to total internal energy [13].

3.2 Material modeling using concrete damage plasticity

The Concrete Damage Plasticity (CDP) constitutive model was used to describe the nonlinear behavior of each component of the small wall (soil-cement brick and mortar joints). The CDP model has been widely used to simulate the behavior of concrete and other brittle materials, such as adobe, tuff, rammed earth, and soil-cement masonry [16][17][18][13]. This constitutive model is capable of modeling the two main failure mechanisms of brick and mortar: tensile cracking and compression crushing.

The CDP model represents the loss of stiffness due to plasticity damage in both compression and tension. Stiffness degradation occurs according to the damage parameters in compression (d_c) and tension (d_t). The range of damage parameters is from 0 to 1, where values of d_c and d_t close to 1 represent imminent degradation of the material stiffness. According to Bui et al. [18] the damage variables should not exceed 0.99, so for the present study, the maximum value for the tensile and compressive damage parameters was adopted as 0.9.

The damage parameters were calculated according to eq. (1) and (2) of the damage model suggested in Birtel and Mark [19]. The Birtel and Mark damage model is defined as a function of E_0, stresses (σ_c and σ_t) and plastic deformations (ε_c^{pl} and ε_t^{pl}). The dimensionless constant factors b_c and b_t vary from 0 to 1, for this study the following were adopted: b_c = 0.75 and b_t = 0.7 for the bricks; b_c = 0.7 and b_t = 0.7 for the adhesive mortar.

$$d_c = 1 - \frac{\sigma_c . E_0^{-1}}{\varepsilon_c^{pl} . (1/b_c - 1) + \sigma_c . E_0^{-1}} \tag{1}$$

$$d_t = 1 - \frac{\sigma_t . E_0^{-1}}{\varepsilon_t^{pl} . (1/b_t - 1) + \sigma_t . E_0^{-1}} \tag{2}$$

The strain components ε_c^{pl} and ε_t^{pl} are obtained from the portion of inelastic deformations (ε_c^{in} and ε_t^{in}) and the factors b_c and b_t according to eq. (3) and (4):

$$\varepsilon_c^{pl} = b_c . \varepsilon_c^{in} \tag{3}$$

$$\varepsilon_t^{pl} = b_t . \varepsilon_t^{in} . \tag{4}$$

According to the ABAQUS user manual [13], the basic parameters of the CDP model are: the expansion angle (ψ), the eccentricity (e), the ratio between the initial biaxial and uniaxial compressive yield stresses (f_{b0} /f_{c0}), the ratio of the second stress invariant in the tensile meridian (K) and the viscosity parameter (υ_p). Table 1 presents the parameters assumed for the calibration of the soil-cement brick and the adhesive mortar, based on the numerical studies developed for soil-cement [13] and concrete block masonry [15].

Table 1. CDP Parameters

Parameters	Soil-cement brick	Adhesive mortar
ψ	10º	40º
e	0.1	0.1
f_{b0} /f_{c0}	1.16	1.16
K	0.667	0.667
υ_p	0.0005	0.0001

3.3 Brick and mortar under uniaxial compression or tension

In addition to the parameters previously highlighted, it is necessary to provide ABAQUS with information on the stress-strain relationships (σ x ε) of each material used, both for tension and compression. Thus, the σ x ε relationship curve for the compression and tension behavior of the materials was determined, taking as reference model of general compression and tension proposed by Guo [20]. This strategy was adopted in studies of concrete [15] and tuff masonry [17]. Figure 3 presents the general compression and tension curve proposed by Guo [20].

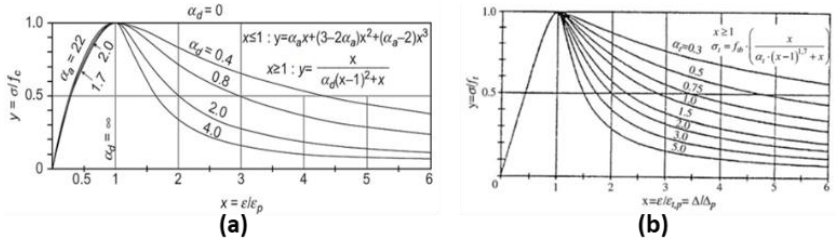

Figure 3. Stress-strain relationship curve: (a) compression; (b) tension [20]

The formulation of the Guo [20] are basically divided into elastic and inelastic regions. The elastic region of the compression and tensile curves are governed by the E_0 defined for the material, while the inelastic region is obtained according to eq. (5), (6), (7) and (8) for the compression curve and eq. (9), (10) and (11) for the tensile behavior curves. In addition to E_0, the model requires the secant modulus related to peak stress (E_p), peak strains (ε_p^c and ε_p^t), compressive and tensile strength (f_c and f_t) and the dimensionless coefficients α_a, α_d and α_t.

$$\sigma_c = f_c \cdot [\alpha_a . x_c + (3 - 2.\alpha_a) . x_c{}^2 + (\alpha_a - 2) . x^3] \rightarrow x_c \leq 1 \tag{5}$$

$$\sigma_c = f_c \cdot \frac{x_c}{\alpha_d \cdot (x_c - 1)^2 + x_c} \rightarrow x_c > 1 \tag{6}$$

$$x_c = \varepsilon_c / \varepsilon_p^c \tag{7}$$

$$\alpha_a = E/E_p, 0.4 \leq \alpha_d \leq 4{,}0 \tag{8}$$

$$\sigma_t = f_t \cdot \frac{x_t}{\alpha_d . (x_t - 1)^{1,7} + x_t} \tag{9}$$

$$x_t = \varepsilon_t / \varepsilon_p^t \tag{10}$$

$$\alpha_t = 0.312 \cdot f_t \tag{11}$$

In the present study, E_0 for soil-cement bricks was adopted as 4000 MPa as suggested by Assis [20], being defined at 30% of f_c of the maximum stress. For the laying mortar, E_0 was adopted as the average of the E_0 calculated at 30% of the maximum stress of the experimental curves. The peak strains for both materials were obtained from the experimental compression curves. The Poisson's ratio adopted for both materials was 0.2 [15][21]. Table 2 presents a summary of the values used in the calibration of the numerical simulation.

Table 2. Properties of soil-cement bricks and adhesive mortars in compression and tension

Material	E_0 (MPa)	Poisson's Ratio	Compression				Tension		
			f_c (MPa)	$\varepsilon_{c,p}$ (10^{-3})	α_a	α_d	f_t (MPa)	$\varepsilon_{t,p}$ (10^{-3})	α_t
Soil-cement brick	4000	0.2	6.5	5	3.08	0.4	0.4	0.1	0.125
Adhesive mortar	2566.7	0.2	15.4	10	1.8	3.5	2.35	0.92	0.705

3.4 Contact properties

For the interfaces between the soil-cement brick components and the adhesive mortar joints, as well as between the upper and lower end plates and the masonry, contact interaction of the hard contact type and the possibility of tangential displacement between the materials were considered. Regarding the tangential behavior of the bricks and joints, a static friction coefficient of 0.6 was adopted, based on the calibrations in Carvalho [14]. For the interface between the rigid plates and the mortar, a friction coefficient of 0.4 was used, as adopted by Leal [15].

4 Comparison between experimental–numerical results

Figure 4 shows contour plots of tensile damage (DAMAGET) compared to the experimental model tested. The initiation of tensile failure during the simulation occurred at the end brick, propagating along the mortar joints of the small wall. Crack propagation was pronounced, with tensile damage spreading along a vertical strip slightly inclined to the application of force. It is noted that he numerical model adequately captured the failure mode of the structure, in terms of tensile damage distribution and crack initiation and propagation.

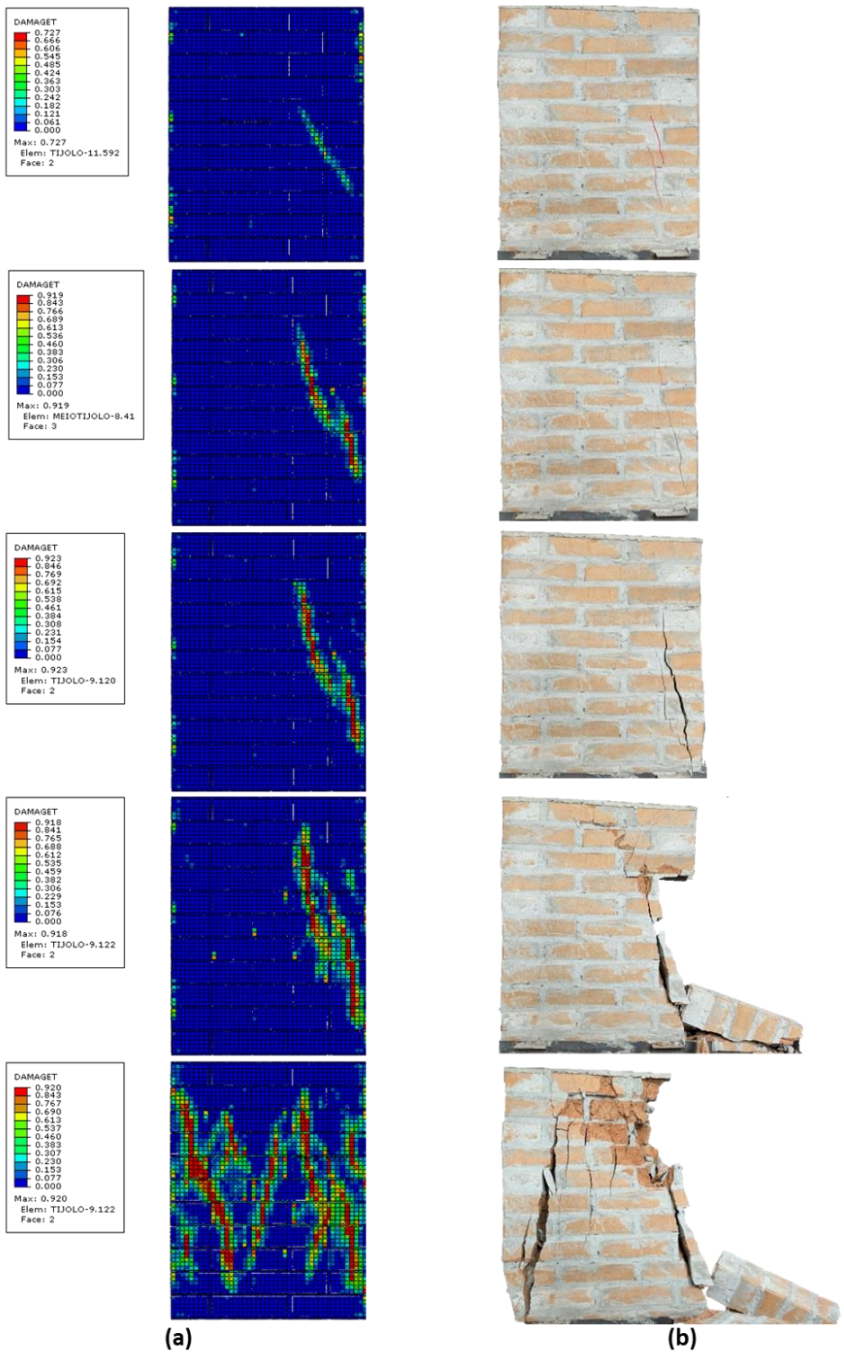

Figure 4. Comparison: (a) tensile damage (numerical); (b) experimental

With the gradual increase in the displacement imposed on the numerical model, the degradation of the material under compression intensified, represented by the damage variable DAMAGEC. With the increase in damage, the decay in the model's resistance capacity became more pronounced (Figure 5). However, it is observed

that as the tensile degradation of the material propagates, the numerical analysis does not fully simulate the crushing at the brick face and upper joints observed in the experimental model.

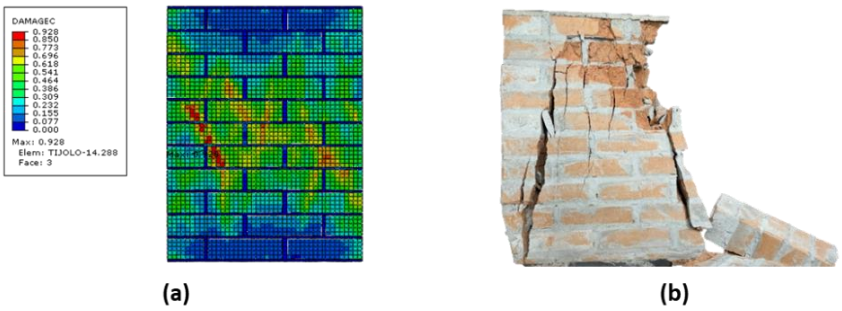

Figure 5. Comparison: (a) compression damage (numerical); (b) experimental

Figure 6 compares the results of the numerical analysis with the stress-strain curves of the vertical LVDTs installed in the six small walls tested. The numerical model is able to predict the load-bearing capacity of the soil-cement masonry, presenting a maximum difference of 2.98% compared to the average of the experimental results. Figure 6-b shows that the numerical model in the inelastic regime, before the peak stress, is less deformed than most of the curves of the experimental models. However, it is noted that the stress-strain curve of the numerical analysis is within the limits of the experimental envelopes.

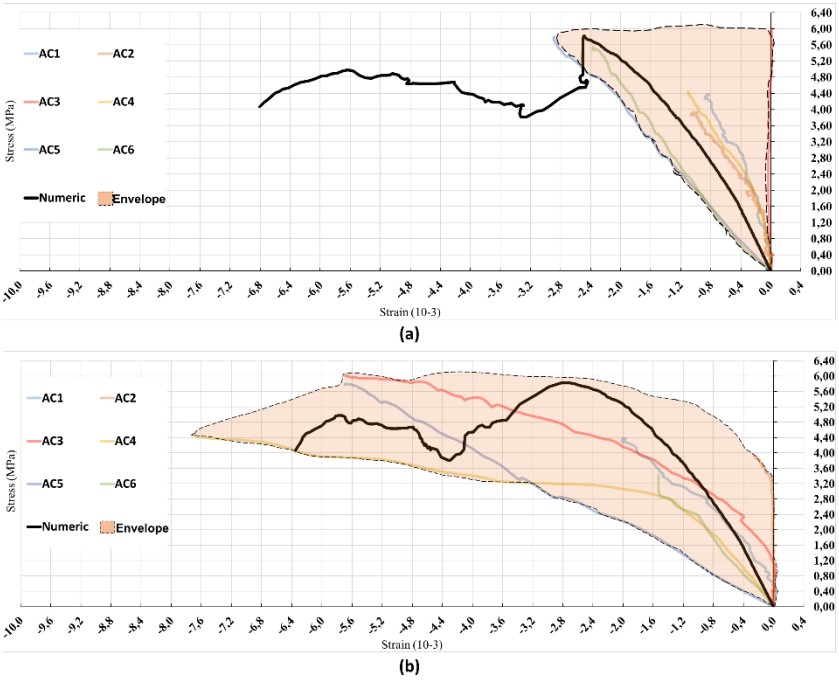

Figure 6. Stress-Strain curves of small walls: (a) left side; (b) right side

5 Conclusions

The numerical simulation performed in this work showed good accuracy. The CDP constitutive model, the Guo curve model and the Birtel and Mark damage model adopted proved to be adequate to simulate the mechanical behavior of small soil-cement walls with adhesive mortar joints.

It is consolidated that the numerical model used in this study, although it was constructed with some geometric-mechanical simplifications in relation to the real conditions of the experimental analysis that incorporates a series of variables, managed to provide a valid approximation for the global behavior of the

structure, including the compression capacity of the small walls, the spreading of cracks and the concentration of damage to compression and tension. In general, the numerical curve obtained was between the experimental curves.

Acknowledgements. The authors would like to thank FAPEMIG, CAPES, CNPq, PROPEEs and UFMG for providing the resources and support necessary for the preparation of this scientific article.

Authorship statement. The authors hereby confirm that they are the sole liable persons responsible for the authorship of this work, and that all material that has been herein included as part of the present paper is either the property (and authorship) of the authors, or has the permission of the owners to be included here.

References

[1] N. Tarque, M Blondet, J. Vargas-Neumann and R. Yallico-Luque. "Rope mesh as a seismic reinforcement for two-storey adobe buildings". *Bulletin of Earthquake Engineering*, v. 20, n. 8, p. 3863–3888, 1 july 2022.
[2] P. Kasinikota and D. D. Tripura. "Prediction of physical-mechanical properties of hollow interlocking compressed unstabilized and stabilized earth blocks at different moisture conditions using ultrasonic pulse velocity". *Journal of Building Engineering*, v. 48, p. 103961, 1 may 2022.
[3] M. S. Islam, Tausif-E-Elahi, A. R. Shahriar, K. Nahar and T. R. Hossain. "Strength and Durability Characteristics of Cement-Sand Stabilized Earth Blocks". *Journal of Materials in Civil Engineering*, v. 32, n. 5, p. 04020087, 27 feb. 2020.
[4] G. Mohamad, E. Rizzarri and H. R. Roman. "Modo de ruptura, deformabilidade e resistência de pequenas paredes estruturais". *Ambiente Construído*, vol.11, n.3, p.7-22. Porto Alegre, 2011.
[5] W. I. Villiers. "Computational and Experimental Modelling of Masonry Walling towards Performance-Based Standardisation of Alternative Masonry Units for Low-Income Housing". PhD thesis, *South Africa: Faculty of Engineering, at Stellenbosch University*, dec. 2019.
[6] H. Ma, Q. Ma and P. GAIRE. "Development and mechanical evaluation of a new interlocking earth masonry block." *Advances in Structural Engineering*, v. 23, n. 2, p. 234–247, 8 aug. 2019.
[7] German Institute for Standardisation, "DIN 18945, Earth blocks - Requirements, test and labelling", DIN, 2018.
[8] British Standard Institution, "EN 772-6, Methods of Test for Masonry Units Determination of Bending Tensile Strength of Aggregate Concrete Masonry Units", BS EN, 2001.
[9] K. Huamani, R. Enciso, M. Gonzales, D. Zavaleta and R. Aguilar. "Experimental and numerical evaluation of a stackable compressed earth block masonry system: Characterization at cyclic shear loads". *Journal of Building Engineering*, v. 60, p. 105-139, 15 nov. 2022.
[10] Associação Brasileira De Normas Técnicas, "ABNT NBR 13276: Argamassas para assentamento e revestimento de paredes e tetos – Determinação do índice de consistência", Rio de Janeiro, 2016.
[11] Associação Brasileira De Normas Técnicas, "ABNT NBR 16868-3 - Alvenaria estrutural - Parte 3 - Métodos de ensaio", Rio de Janeiro, 2020c.
[12] P. J. B. B. Lourenço. "Computational Strategy for Masonry Structures". *Netherlands: Delft University of Technology*, 19 feb. 1996.
[13] Dassault Systemes. SIMULIA Abaqus Analysis User's Manual Version 6.14, 2014.
[14] P. R. O. Carvalho, D. F. Leal and J. M. Neto. "Análise numérica de pequenas paredes de alvenaria estrutural de blocos de concreto em situação de incêndio". Matéria (Rio de Janeiro), v. 26, n. 3, 11 oct. 2021.
[15] D. F. Leal. "Análise experimental e numérica sobre alvenaria estrutural de blocos de concreto, com e sem revestimento, em situação de incêndio". PhD thesis, *Brasil: Escola de Engenharia de São Carlos, Universidade de São Paulo*, dec. 2022.
[16] R. Illampas, D. C. Charmpis ans I. Ioannou. "Laboratory testing and finite element simulation of the structural response of an adobe masonry building under horizontal loading". *Engineering Structures*, v. 80, p. 362-376, 1 dec. 2014.
[17] E. Nastri, M. Tenore, P. Todisco. "Calibration of concrete damaged plasticity materials parameters for tuff masonry types of the Campania area". *Engineering Structures*, v. 283, 15 may 2023.
[18] T. L. Bui, T. T. Bui, Q. B. Bui, X. H. Nguyen, A. Limam. "Out-of-plane behavior of rammed earth walls under seismic loading: Finite element simulation". *Structures*, v. 24, 24 apr. 2020.
[19] V. Birtel and P. Mark. "Parameterised finite element modelling of rc beam shear failure". *ABAQUS Users' Conference*, p.95-108, 2006.
[20] Z. Guo. "Principles of reinforced concrete". First edition. *USA: Elsevier*, 587p., 2014.
[21] J. B. S. Assis. "Determinação experimental da resistência à Tração na flexão em paredes construídas com Blocos encaixáveis de solo-cimento". PhD thesis, *Brasil: Escola de Engenharia de Universidade Federal de Minas Gerais*, jun. 2006.
[22] J. A. Cottrell, M. Ali, A. Tatari, D. B. Martinson. "An investigation into the influence of geometry on compressed earth building blocks using finite element analysis". *Construction and Building Materials*, v. 273, 1 mar. 2021.